



HAL
open science

Preliminary analysis of CH₃D from 3250 to 3700 cm⁽⁻¹⁾

Andrei Nikitin, Jean-Paul Champion, Linda R. Brown

► **To cite this version:**

Andrei Nikitin, Jean-Paul Champion, Linda R. Brown. Preliminary analysis of CH₃D from 3250 to 3700 cm⁽⁻¹⁾. *Journal of Molecular Spectroscopy*, 2006, 240, pp.14-25. 10.1016/j.jms.2006.08.002 . hal-00273107

HAL Id: hal-00273107

<https://hal.science/hal-00273107>

Submitted on 22 Apr 2011

HAL is a multi-disciplinary open access archive for the deposit and dissemination of scientific research documents, whether they are published or not. The documents may come from teaching and research institutions in France or abroad, or from public or private research centers.

L'archive ouverte pluridisciplinaire **HAL**, est destinée au dépôt et à la diffusion de documents scientifiques de niveau recherche, publiés ou non, émanant des établissements d'enseignement et de recherche français ou étrangers, des laboratoires publics ou privés.

Preliminary analysis of CH₃D from 3250 to 3700 cm⁻¹

A.V. Nikitin^a, J.-P. Champion^b and L.R. Brown^c

^aLaboratory of Theoretical Spectroscopy, Institute of Atmospheric Optics, Russian Academy of Sciences, 634955 Tomsk, Russia.

^bLaboratoire de Physique de l'Université de Bourgogne, UMR CNRS 5027, 9 Avenue A. Savary, BP 4780, F-21078 Dijon Cedex, France.

^cJet Propulsion Laboratory, California Institute of Technology, 4800 Oak Grove Drive, Pasadena, CA 91109, USA.

Abstract

The infrared spectrum of CH₃D from 3250 to 3700 cm⁻¹ was studied for the first time to assign transitions involving the $\nu_2 + \nu_3$, $\nu_2 + \nu_5$, $\nu_2 + \nu_6$, $\nu_3 + 2\nu_6$ and $3\nu_6$ vibrational states. Line positions and intensities were measured at 0.011 cm⁻¹ resolution using Fourier transform spectra recorded at Kitt Peak with isotopically enriched samples. Some 2852 line positions (involving over 900 upper state levels) and 874 line intensities were reproduced with RMS values of 0.0009 cm⁻¹ and 4.6%, respectively. The strongest bands were found to be $\nu_2 + \nu_3$ at 3499.7 cm⁻¹ and $\nu_2 + \nu_6$ at 3342.5 cm⁻¹ with integrated strengths, respectively, of 8.17×10^{-20} and 2.44×10^{-20} (cm⁻¹/molecule · cm⁻²) at 296 K (for 100% CH₃D). The effective Hamiltonian was expressed in terms of irreducible tensor operators and adapted to symmetric top molecules. Its present configuration in the MIRS package permitted simultaneous consideration of the four lowest polyads of CH₃D: the Ground State (G.S.), the Triad from 6.3 to 9.5 μ m, the Nonad from 3.1 to 4.8 μ m and now the Enneadecad (19 bands) from 2.2 to 3.1 μ m. The CH₃D line parameters for this interval were calculated to create a new database for the 3 μ m region.

Keywords : CH₃D; Monodeuterated methane; Hot bands; Line positions; Line intensities; Database Article Outline

Contents

1	Introduction	3
2	Experimental details	6
3	Theoretical framework	7
4	Results and discussion	8
4.1	Positions and energy levels	9
4.2	Intensity fit	10
5	Database of line parameters	11
6	Conclusion	12

List of Tables

1	CH ₃ Dgas sample conditions	6
2	Overview of the CH ₃ D Enneadecad model	7
3	Summary of the CH ₃ D energy level fit	8
4	Effective transition moment terms for the Enneadecad 12CH ₃ D (in Debye)	8
5	Summary of the CH ₃ D intensity fit	9

List of Figures

1	Observed absorption spectrum of the CH ₃ D from 3000 to 5000 cm ⁻¹	3
2	Vibrational structure of CH ₃ D.	4
3	Reduced energy diagram of the CH ₃ D Enneadecad.	5
4	Observed absorption spectrum of the CH ₃ D	6
5	Observed intensity diagram of CH ₃ D.	10
6	Simulated absorption spectrum of CH ₃ D in the Lower Enneadecad region.	12

1 Introduction

Monodeuterated methane (CH_3D) is often used to determine the H/D ratios in planetary atmospheres [1] and [2]. The $3\ \mu\text{m}$ region is important for outer planet studies because it is a “window” free of strong CH_4 absorption [3]. New observations from spacecraft (such as VIMS [4] on Cassini), aircraft platforms (such as SOFIA [5]) and high-resolution ground-based telescopes [6] have revealed the need for $3\ \mu\text{m}$ CH_3D line parameters because its features can overlap those of other planetary molecules such as NH_3 , PH_3 , HCN , C_2H_2 and C_2H_6 .

Appropriate theoretical models for such symmetric tops [7] and [8] are already available from formalisms developed for spherical rotors [9] and [10]. Accurate representation of the positions and intensities of this molecule requires that the polyad scheme be used. The six fundamentals of CH_3D are grouped into two polyads; the Triad ($6\text{--}10\ \mu\text{m}$) is composed of the three lowest fundamentals (ν_6 , ν_3 , ν_5) [11] while the Nonad ($3\text{--}5\ \mu\text{m}$) contains the three upper fundamentals (ν_2 , ν_4 , ν_1) with three combination bands ($\nu_3 + \nu_6$, $\nu_5 + \nu_6$, $\nu_3 + \nu_5$) and three overtones ($2\nu_6$, $2\nu_3$, $2\nu_5$) [12]. The common effective Hamiltonian is developed so that vibrational states within each polyad can be treated simultaneously in order to account for numerous interactions between the energy levels.

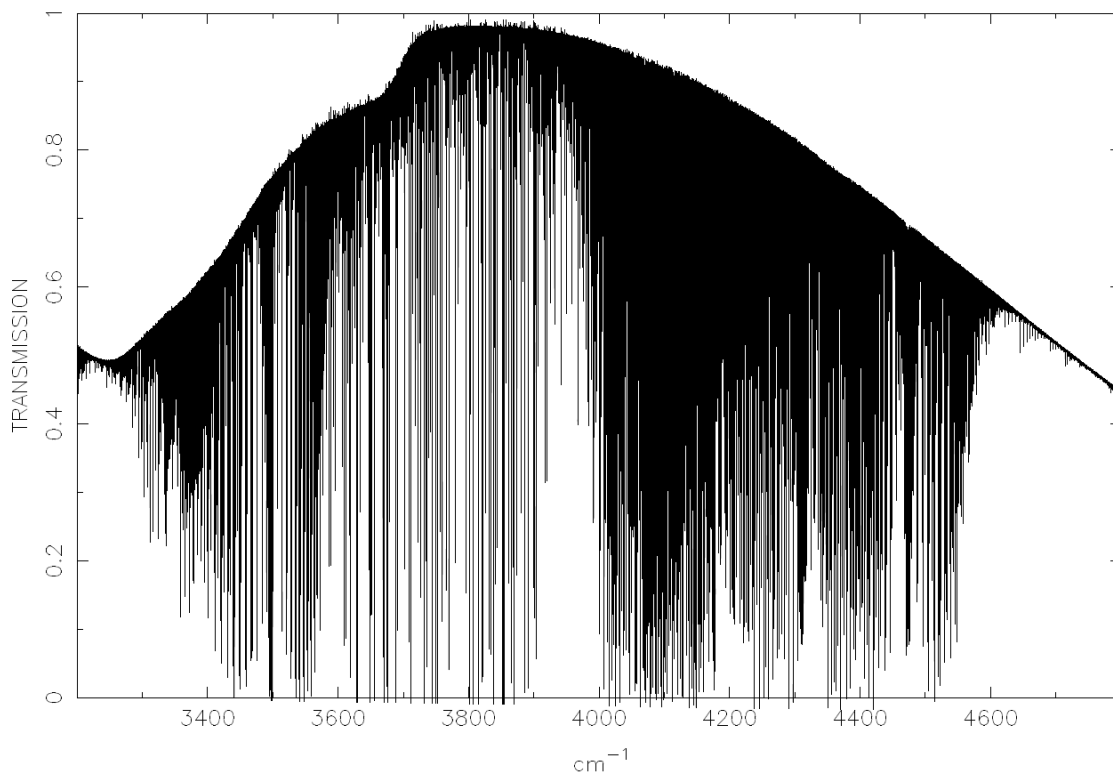


Figure 1: Observed absorption spectrum of the CH_3D from 3000 to $5000\ \text{cm}^{-1}$.

The vertical axis is on an arbitrary scale. The optical path is $150\ \text{cm}$, and the pressure is $20\ \text{torr}$ with a 98% enriched sample at $294\ \text{K}$. The scan was recorded in a $70\ \text{min}$ period at $0.012\ \text{cm}^{-1}$ resolution using the McMath-Pierce FTS at Kitt Peak. The full bandpass of the spectrum is from 1850 to $5200\ \text{cm}^{-1}$. The 19 bands of the Enneadecad fall in the interval from 3200 to $4800\ \text{cm}^{-1}$. The strong features between 3650 and $3950\ \text{cm}^{-1}$ due to residual H_2O mask the four weakest CH_3D bands. The features near $3000\ \text{cm}^{-1}$ are the upper portion of the Nonad.

The CH_3D spectrum between 2.2 and $3\ \mu\text{m}$ has not been studied previously partly because the region is so complicated. In Fig. 1, a laboratory spectrum is shown between 3000 and $5000\ \text{cm}^{-1}$. The spectral interval has a polyad of 19 interacting states of CH_3D and is designated as the Enneadecad. Its bands are essentially the Triad quanta combined with the Nonad states: $\nu_1 + \nu_3$, $\nu_1 + \nu_5$, $\nu_1 + \nu_6$, $\nu_2 + \nu_3$, $\nu_2 + \nu_5$, $\nu_2 + \nu_6$, $\nu_3 + \nu_4$, $\nu_4 + \nu_5$, $\nu_4 + \nu_6$, $3\nu_3$, $2\nu_3 + \nu_5$, $2\nu_3 + \nu_6$, $\nu_3 + 2\nu_5$, $\nu_3 + \nu_5 + \nu_6$, $\nu_3 + 2\nu_6$, $3\nu_5$, $2\nu_5 + \nu_6$, $\nu_5 + 2\nu_6$ and $3\nu_6$. These 19 vibrational states are in fact comprised of 37 separate vibrational sublevels, most of which ultimately give rise to infrared absorption from the ground state. Although the Enneadecad of CH_3D corresponds to the Octad of CH_4 from 2.1 to $2.8\ \mu\text{m}$ [13], the

detailed comparison of corresponding bands is not obvious. The Enneadecad of CH_3D contains 12, 7 and 18 sublevels of symmetry A_1 , A_2 and E , respectively, while the Octad of CH_4 contains 4, 2, 5, 5, 8 sublevels of symmetry A_1 , A_2 , E , F_1 , F_2 , respectively. In both cases the overall vibrational degeneracy is 55.

The complexity of the Enneadecad states is illustrated in Fig. 2. This schematic shows the 19 vibrational levels designated by the number of quanta for each fundamental $\nu_1, \nu_2, \nu_3, \nu_4, \nu_5, \nu_6$ (e.g., 010001 is $\nu_2 + \nu_6$, 011000 is $\nu_2 + \nu_3$ and 000003 is $3\nu_6$). The vibrational symmetry of $\nu_2 + \nu_5$ and $\nu_2 + \nu_6$ is E , while $\nu_2 + \nu_3$ is A_1 . The states drawn with doubled lines have multiple sub-components; for example, $3\nu_6$ has three (A_1 , A_2 and E) sub-levels, and $\nu_3 + 2\nu_6$ has two (A_1 and E). The vibrations are redrawn in the three other columns to show the expected Fermi and Coriolis interactions based on prior studies of the Triad [11] and Nonad [12]. As a preliminary approach, the Enneadecad polyad can be grouped into three sets. The lowest section between 3250 and 3700 cm^{-1} contains five bands which are essentially the Triad plus ν_2 or $2\nu_6$ ($\nu_2 + \nu_6$, $3\nu_6$, $\nu_2 + \nu_3$, $\nu_3 + 2\nu_6$ and $\nu_2 + \nu_5$) while the upper portion between 4000 and 4700 cm^{-1} has 10 bands (Triad plus upper Nonad: $2\nu_3 + \nu_5$, $2\nu_5 + \nu_6$, $\nu_1 + \nu_6$, $\nu_4 + \nu_6$, $\nu_3 + 2\nu_5$, $\nu_1 + \nu_3$, $\nu_3 + \nu_4$, $3\nu_5$, $\nu_1 + \nu_5$ and $\nu_4 + \nu_5$). The middle set of four bands from 3700 to 4000 cm^{-1} ($2\nu_3 + \nu_6$, $\nu_5 + 2\nu_6$, $3\nu_3$ and $\nu_3 + \nu_5 + \nu_6$) all involve three quanta of the Triad excited states and are thus expected to be much weaker than the “two quanta” bands in the upper and lower intervals. In our laboratory spectra, only weaker transitions with intensity stronger than 5×10^{-24} ($\text{cm}^{-1}/\text{molecule} \cdot \text{cm}^{-2}$) are visible, and so the lines in the middle part are not generally observed.

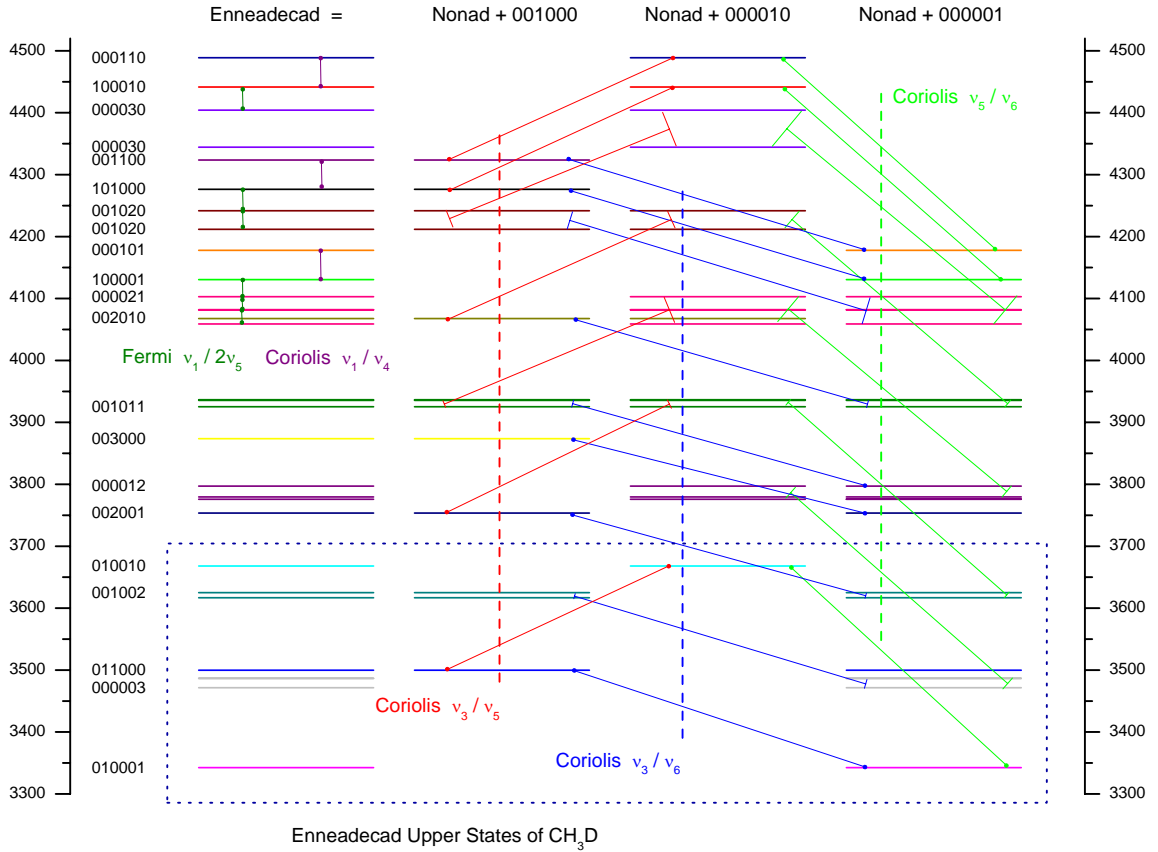


Figure 2: Vibrational structure of CH_3D .

Vibrational structure of $^{12}\text{CH}_3\text{D}$ energy levels with dominant Fermi and Coriolis couplings extrapolated from Triad and Nonad that are required to model the 19 bands of the Enneadecad. Higher order interactions are not indicated. The vibrational levels are indicated as $\nu_1\text{--}\nu_6$.

In this article, only the five lowest bands of the Enneadecad are directly analyzed because of the immediate usefulness to planetary astronomy. With the theoretical model, it is possible to predict the approximate location of upper state energy levels as shown in Fig. 3. In the upper panel, the predicted values of reduced upper state energy levels in cm^{-1} are plotted vs the upper state J (the lower panel has the levels that have been assigned in the present

study).

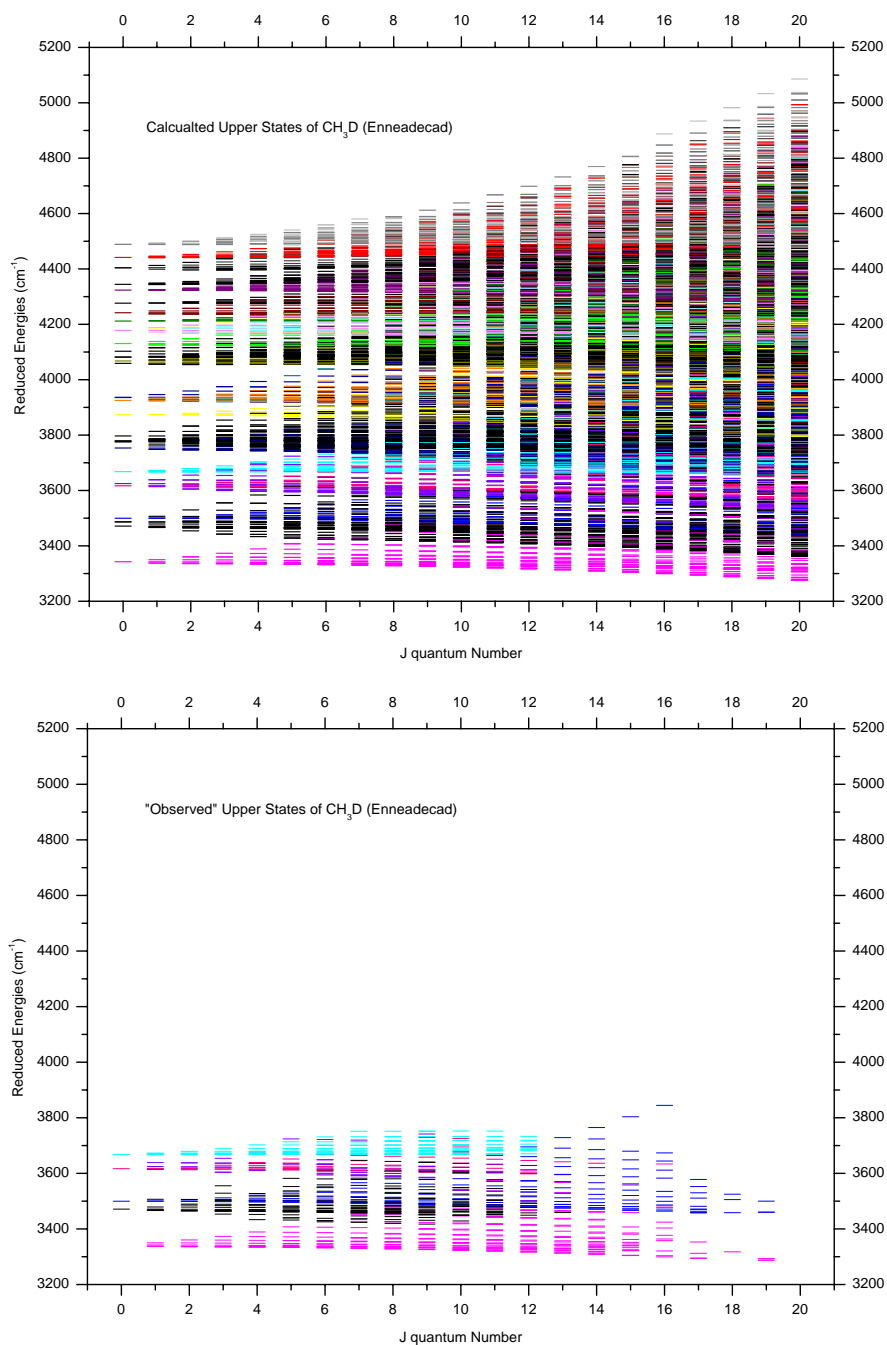


Figure 3: Reduced energy diagram of the CH_3D Enneadecad.

Reduced upper state energies in cm^{-1} versus upper state J for the nineteen bands of the $^{12}\text{CH}_3\text{D}$ Enneadecad between 3000 and 4800 cm^{-1} . The upper panel shows the calculated levels, and the lower panel shows the observed levels. The colors reflect the complexity of the vibrational mixing of the states. No detailed coding is given due to the large number of vibrational components to be distinguished.

Many of the interactions between the observed states and the higher sub-vibrational levels are nevertheless included in the model because we used as fixed constants the corresponding interactions within the Triad and Nonad. The vibrational pattern of the entire Enneadecad shown on the upper panel of Fig. 3 illustrates how the main Coriolis and Fermi interactions are extrapolated from the Triad and the Nonad. In particular, the lower Enneadecad has interactions with the middle part due to strong Coriolis terms already known from our previous analysis of the Triad. Similarly the interaction terms active in the Nonad also apply to corresponding states of the Enneadecad. The major

advantage of our model is that all the terms and corresponding constants (diagonal or not) obtained in our previous analyses of the lower polyads (Triad and Nonad) can be directly included in the Enneadecad model. In the present work, all major interactions within the Enneadecad are thus considered. This provides an excellent starting prediction for assigning the unexplored region. One interesting aspect of the present study is to discern effects of higher order interactions between the lower and middle portions of the Enneadecad.

2 Experimental details

Table 1: CH₃D gas sample conditions

Pressure (Torr / Pa)	Path Length (m)	Temperature (K)
1800 to 5500 cm ⁻¹ bandpass at 0.011 cm ⁻¹ resolution		
15.50 / 2070	0.10	294.3
4.50 / 600	0.25	295.8
9.73 / 1300	0.25	295.9
0.72 / 96	2.39	291.0
4.88 / 650	2.39	291.0
20.0 / 3200	1.50	294.9
40.2 / 5360	1.50	294.9
89.6 / 11900	1.50	295.6

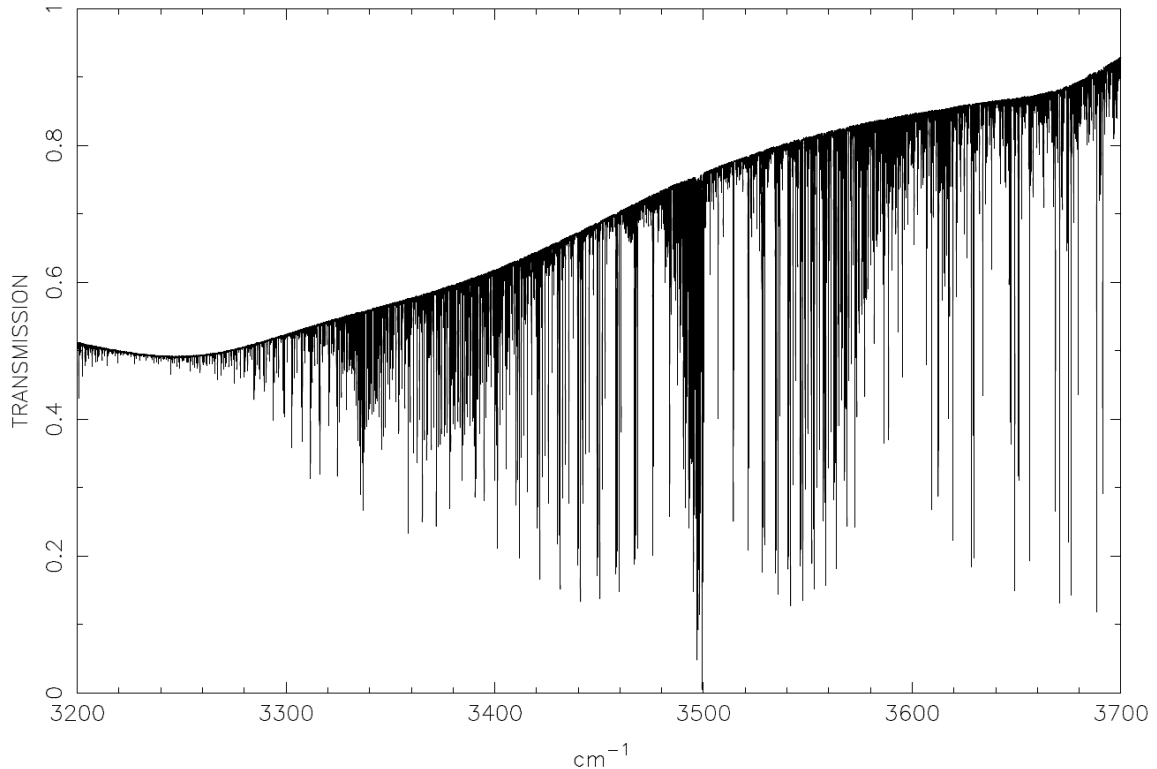


Figure 4: Observed absorption spectrum of the CH₃D

Observed absorption spectrum of the CH₃D from Fig. 1 in the region analyzed here. The vertical axis is on an arbitrary scale. The two prominent bands are $\nu_2 + \nu_6$ (3350 cm⁻¹) and $\nu_2 + \nu_3$, (3500 cm⁻¹). The region also contains $3\nu_6$ (3480 cm⁻¹), $\nu_3 + 2\nu_6$ (3620 cm⁻¹) and $\nu_2 + \nu_5$ (3680 cm⁻¹). The strongest lines between 3600 and 3700 cm⁻¹ are due to residual water.

The spectral data for the present study came from our previous analysis of the Nonad [12], and so experimental details are only briefly repeated here. The spectra were recorded at 0.011 cm^{-1} resolution using the McMath-Pierce Fourier Transform Spectrometer configured with InSb detectors. The spectral band pass covered both the Nonad and the present region simultaneously. Enneadecad positions and intensities at $3 \mu\text{m}$ could be measured in eight spectra; these involved pure samples of 98%-enriched CH_3D at room temperature in five different absorption cells (with optical paths ranging from 10 to 239 cm). The gas sample conditions are shown in Table 1, and an expanded spectral plot of the measured region is shown in Fig. 4.

The line positions were initially obtained by peak finding of the apodized spectra and later by curve-fitting of the unapodized spectra. The measured line positions and intensities were retrieved using nonlinear-least squares [14] in which the parameters of a synthetic spectrum were adjusted to minimize the differences between observed and calculated spectra; for the higher pressure data, self-broadened widths were also adjusted (but are not being reported). Parameters of residual water features were also adjusted if water transitions fell near the targeted CH_3D lines. Measurements from different spectra were then combined and averaged to produce the observed values. Examples of this process are shown in the earlier studies of the Triad [11] and Nonad [12]. The accuracies of the intensities depended on the determination of the enriched abundance (1%), as well as the usual uncertainties of the measured pressures (1%), optical path lengths (0.2–2%) and temperature (0.5–2 K). The present measured intensities are reported for 100% CH_3D with precisions of $\pm 3\%$.

The calibration of the wavenumber (cm^{-1}) scale obtained for the Nonad [12] using the 1-0 band of CO [15] was applied to the bands at $3 \mu\text{m}$. The precisions are generally $\pm 0.0004 \text{ cm}^{-1}$ for line positions of well-isolated features obtained from the lower pressure spectra. However, positions of the weakest lines taken from the scans at 40 and 90 torr are pressure shifted, but no corrections have been attempted because the present data do not permit accurate self-broadened shifts to be measured. Based on studies of CH_3D fundamentals [16 and the references therein] and the expectation that shifts are roughly proportional to the line position, the self-broadened pressure-induced shifts at $3 \mu\text{m}$ could be as large as -0.0015 cm^{-1} with the gas sample at 90 torr. However, the self-shifts vary too greatly as a function of the rotational quanta from band to band to make accurate corrections by extrapolating measurements of the lower fundamentals [16].

3 Theoretical framework

Table 2: Overview of the CH_3D Enneadecad model

Parameter set	Number of energy level parameters	Number of intensity parameters
Whole Polyad 19 states	4621	185
Lower set 5 states	256	58
Lower set of 5 bands determined here	151 + 2 (54 diagonal, 99 off-diagonal)	22
Ratio: number of fitted data to adjusted constants	2852/153 = 18.6	874/22 = 39.7

The theoretical framework of the present work is the same as the one already described in our previous reports [11] and [12]. Only basic or new features will be repeated or detailed here. The partially transformed ro-vibrational Hamiltonian adapted to the polyad structure of the CH_3D molecule is expressed as

$$H = H_{G.S.} + H_{Triad} + H_{Nonad} + H_{Enneadecad} + \dots \quad (1)$$

where the subsequent terms correspond to successive polyads with increasing vibrational energies. The effective Hamiltonians associated with the subsequent polyads includes one, two or three sets of terms obtained by projection of the above equation onto the corresponding subspaces denoted by $\langle Polyad \rangle$:

$$H^{\langle G.S. \rangle} = H_{G.S.}^{\langle G.S. \rangle} \quad (2)$$

$$H^{\langle Triad \rangle} = H_{G.S.}^{\langle Triad \rangle} + H_{Triad}^{\langle Triad \rangle} \quad (3)$$

$$H^{(Nonad)} = H_{G.S.}^{(Nonad)} + H_{Triad}^{(Nonad)} + H_{Nonad}^{(Nonad)} \quad (4)$$

$$H^{(Enneadecad)} = H_{G.S.}^{(Enneadecad)} + H_{Triad}^{(Enneadecad)} + H_{Nonad}^{(Enneadecad)} + H_{Enneadecad}^{(Enneadecad)} \quad (5)$$

In the present work, the parameters from $H_{G.S.}$ involved in the effective Hamiltonians for the three polyads (ground state, Triad and Nonad) through the respective terms $H_{G.S.}^{(G.S.)}$, $H_{G.S.}^{(Triad)}$, $H_{G.S.}^{(Nonad)}$, $H_{G.S.}^{(Enneadecad)}$ were kept fixed at the values reported by Ulenikov et al. [17]. The parameters from H_{Triad} and H_{Nonad} involved in Triad, Nonad and Enneadecad effective Hamiltonians were kept fixed at the values reported in [12]. The dipolar transition moment was similarly expressed in tensorial form. It is partially transformed according to the polyad scheme of the CH₃D molecule. In the present paper, only the Enneadecad-G.S. system is considered, formally expressed as $M^{(GS;Enneadecad)}$ [8].

4 Results and discussion

Table 3: Summary of the CH₃D energy level fit

Energy level	Origin (cm ⁻¹)	Total # of fitted pos.	# from cold bands	# from hot bands	RMS (cm ⁻¹)	Max J(K)
v2 + v3	3499.717	564	382	182	0.0008	18(16)
v2 + v5	3668.076	486	261	225	0.0011	12(9)
v2 + v6	3342.572	931	514	417	0.0009	18(15)
v3 + 2v6 (A1)	3616.791	184	152	32	0.0013	14(9)
v3 + 2v6 (E)	3625.011	96	90	6	0.0015	13(8)
3v6 (A1)	3486.449	40	8	32	0.0011	10(6)
3v6 (A2)	3486.717	75	31	44	0.0009	11(9)
3v6 (E)	3471.464	476	218	258	0.0009	3(10)

Table 4: Effective transition moment terms for the Enneadecad 12CH₃D (in Debye)

	Tensorial nomenclature			Parameter value	
	Rotational	Vibrational	Symm. RV	Computer input	Rounded (St.Dev.)
1	R0(0,0A ₁)	000000 011000	A ₁	-2.6430547653×10 ⁻³	-2.6430(36)×10 ⁻³
2	R0(0,0A ₁)	000000 001002	A ₁	9.8764234880×10 ⁻⁵	9.87(43)×10 ⁻⁵
3	R0(0,0A ₁)	000000 000003	A ₁	1.1894648156×10 ⁻⁴	1.189(63)×10 ⁻⁴
4	R0(0,0A ₁)	000000 010010	E	1.1074517419×10 ⁻³	1.1074(25) ×10 ⁻³
5	R0(0,0A ₁)	000000 010001	E	-1.8878218258×10 ⁻³	-1.8878(43)×10 ⁻³
6	R0(0,0A ₁)	000000 001002	E	4.8403868533×10 ⁻⁴	4.840(53)×10 ⁻⁴
7	R0(0,0A ₁)	000000 000003	E	-6.9197350621×10 ⁻⁴	-6.919(25)×10 ⁻⁴
8	R1(1,1E)	000000 010001	A ₁	9.1542588248×10 ⁻⁶	9.15(13)×10 ⁻⁶
9	R1(1,0A ₂)	000000 000003	A ₁	-9.1058766334×10 ⁻⁶	-9.1(12) ×10 ⁻⁶
10	R1(1,1E)	000000 000003	A ₁	-1.8323611344×10 ⁻⁵	-1.832(28)×10 ⁻⁵
11	R1(1,1E)	000000 011000	E	8.1406663845×10 ⁻⁶	8.14(36)×10 ⁻⁶
12	R1(1,1E)	000000 010010	E	-1.6053578327×10 ⁻⁵	-1.605(50)×10 ⁻⁵
13	R1(1,0A ₂)	000000 010001	E	-1.8723554740×10 ⁻⁵	-1.872(23)×10 ⁻⁵
14	R1(1,1E)	000000 000003	E	-6.4553297042×10 ⁻⁶	-6.45(71)×10 ⁻⁶
15	R1(1,0A ₂)	000000 000003	E	8.1822125751×10 ⁻⁶	8.18(37)×10 ⁻⁶
16	R1(1,1E)	000000 000003	E	-7.9466504387×10 ⁻⁶	-7.9(12) ×10 ⁻⁶
17	R2(2,1E)	000000 010010	A ₁	8.4986120166×10 ⁻⁷	8.49(32) ×10 ⁻⁷
18	R2(2,2E)	000000 010010	A ₁	1.2113159126×10 ⁻⁷	1.21(45) ×10 ⁻⁷
19	R2(2,1E)	000000 010001	A ₁	-1.1137393657×10 ⁻⁷	-1.11(11) ×10 ⁻⁷
20	R2(2,1E)	000000 011000	E	2.3606206413×10 ⁻⁷	2.36(22) ×10 ⁻⁷
21	R2(0,0A ₁)	000000 010001	E	7.6583197022×10 ⁻⁸	7.6(16) ×10 ⁻⁸
22	R2(2,0A ₁)	000000 010001	E	-6.1750844113×10 ⁻⁸	-6.1(16) ×10 ⁻⁸

Starting with the best possible prediction, transitions of the lower Enneadecad were systematically identified. Some assignments were confirmed and extended by considering corresponding transitions of the Enneadecad–Triad difference bands in the ν_2 and $2\nu_6$ region at 4.5 μm . Positions in both regions were modeled together. Then observed line intensities were retrieved from the spectra and fitted to the model. Table 2 and Table 3 provide overviews of the fitting; Table 4 lists the adjusted transition moment parameters, and Table 5 has the statistics of the intensity fit and intensity summations. The Appendix A contains the Hamiltonian constants from the positions fit. Complete files of non-truncated parameters adapted to the computer package MIRS4 [8] are available on <http://www.iao.ru/mirs/mirs.htm> or <http://www.u-bourgogne.fr/LPUB/mirs.html>. The fitted positions and intensities are places as Supplemental files.

Table 5: Summary of the CH_3D intensity fit

Band	Number of fitted intensities	Max J(K)	RMS (%)	Number of calculated lines	Intensity ^a band sum
$\nu_2 + \nu_3$ (A1)	260	17(13)	3.5	847	81.7
$\nu_2 + \nu_5$ (E)	125	12(9)	5.2	1516	8.29
$\nu_2 + \nu_6$ (E)	372	17(12)	4.1	1615	24.4
$\nu_3 + 2\nu_6$ (A1)	9	4(2)	3.8	684	4.12
$\nu_3 + 2\nu_6$ (E)	6	7(2)	12.2	1357	2.69
$3\nu_6$ (A1)	1	8(1)	11.4	486	0.29
$3\nu_6$ (A2)	6	4(4)	5.8	234	0.5
$3\nu_6$ (E)	95	11(10)	6.4	1285	3.09
$\nu_2 + \nu_3 - \nu_3$				510	1.08
$\nu_2 + \nu_5 - \nu_5$				846	1.08
$\nu_2 + \nu_6 - \nu_6$				1276	5.97
$\nu_3 + 2\nu_6(\text{A1}) - \nu_3$				400	0.48
$\nu_3 + 2\nu_6(\text{A1}) - \nu_6$				113	0.02
$\nu_3 + 2\nu_6(\text{E}) - \nu_3$				394	0.11
$\nu_3 + 2\nu_6(\text{E}) - \nu_6$				227	0.04
$3\nu_6(\text{A1}) - \nu_6$				517	0.28
$3\nu_6(\text{A2}) - \nu_6$				291	0.23
$3\nu_6(\text{E}) - \nu_6$				1435	1.76

Intensity sums for all the weak bands are only approximate. ^aIntensities are in units of 10–21 ($\text{cm}^{-1}/\text{molecule} \cdot \text{cm}^{-2}$) at 296 K for 100% CH_3D

4.1 Positions and energy levels

As seen in Table 2, for the whole polyad $H_{\text{Enneadecad}}$, there are in principle 4621 symmetry allowed terms in the Hamiltonian expansion up to the sixth order of approximation. If only the lower Enneadecad is considered, this number decreases to 256, and in the present study, our fit of 2852 line positions has yielded a unique set of 153 parameters with 151 of them belonging to the lower Enneadecad. Among the 153 adjusted parameters, the number of vibrationally off-diagonal terms (99) is larger than the number of vibrationally diagonal terms (54). It is worthwhile to emphasize that the ratio of the number of fitted data (2852 transitions up to $J = 18$) over the number of adjusted parameters (153) demonstrates the efficiency of our approach using the global simultaneous treatment as compared to conventional band by band or even polyad by polyad treatments for which the number of variable parameters would be much larger.

A complete parameter set including untruncated values (as input to the computer program) is given in the Appendix A. The tensorial notation is used to identify the parameters, and values are rounded off according to their standard errors quoted in parentheses. Complete files of non-truncated parameters adapted to the computer package MIRS4 [8] are also available upon request from the first two authors.

The 17 Ground State parameters were held to values reported by Ulenikov et al. [17]. Some 424 effective Hamiltonian parameters were fixed throughout the analysis to the already-reported Triad and Nonad values [11] and [12]. Use of available higher order interactions between $\nu_2 + \nu_5 \leftrightarrow 3\nu_6$ and $\nu_3 + 2\nu_6 \leftrightarrow 3\nu_6$ did not improve the fit, and those constants were set to zero. The analysis did require some preliminary consideration of the middle Enneadecad

in order to fit $\nu_2 + \nu_5$ and $\nu_3 + 2\nu_6$ transitions for $K > 8$. As seen in Fig. 2, the only simple perturbation expected for $\nu_3 + 2\nu_6$ (001002) by a “middle state” is through a Fermi interaction with $\nu_3 + \nu_5 + \nu_6$ (001011); no simple interaction with a middle region state is indicated for $\nu_2 + \nu_5$. In the end, the observed higher K perturbations were interpreted to arise from interactions with $2\nu_3 + \nu_6$ (002001) and $\nu_5 + 2\nu_6$ (000012). Better fits at higher K were then obtained by evoking a higher order interaction between $\nu_2 + \nu_5$ at 3668.0 cm^{-1} and $2\nu_3 + \nu_6$ at 3753.4 cm^{-1} . It is clear that $2\nu_3 + \nu_6$ and $\nu_5 + 2\nu_6$ should be very weak and could appear in our data only by borrowing intensity from stronger bands. However, more laboratory spectra with higher optical densities are needed to pursue a better analysis.

Detailed statistics of the fit of line positions are given in Table 3 by upper state level; the columns are the vibrational level, the corresponding band origin ($J = 0$), the number of fitted positions (total, cold band from the ground state, hot bands from the Triad levels), the total rms value for the combined data and the maximum J and K included in the fit. As seen in the table, the search for $3\nu_6 - \nu_6$ transitions proved very important for finding levels of the tertiary band $3\nu_6$. We found that rms values computed separately with hot and cold band data were not significantly different from the values in Table 3.

4.2 Intensity fit

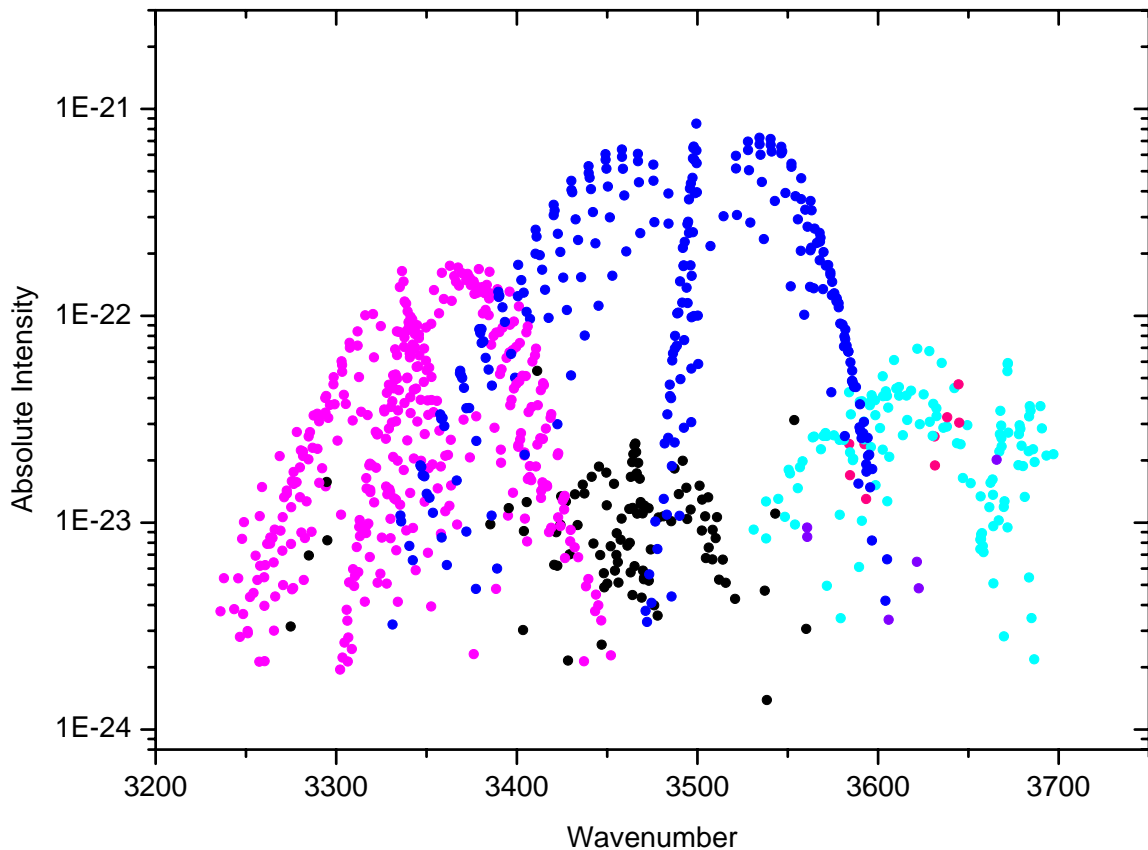


Figure 5: Observed intensity diagram of CH_3D .

Observed intensities in ($\text{cm}^{-1}/\text{molecule} \cdot \text{cm}^{-2}$) at 296 K vs line positions in wavenumber (cm^{-1}) for the 874 CH_3D transitions included in the fit. The corresponding bands are shown above plotted points.

Some 874 empirical intensities up to $J = 18$ were selected from a list of over 1530 measured features and fitted to obtain the intensity parameters for the five lowest bands (with eight sub-components) of the Enneadecad. To indicate the extent of measurements for each band, the observed line intensities are plotted in Fig. 5 as a function of the transition line position. In the model, the effective transition moment of the whole polyad is comprised of 185 symmetry-allowed terms with rotational dependency up to J^2 : these correspond to expansion up to J^2 for two quanta overtones and up

to J for three quanta overtones. Of the 58 that pertain just to the Lower Enneadecad bands, 22 effective parameters were adjusted in order to reproduce the present observed intensities; these are the seven purely vibrational transition moments and 15 J -dependent terms listed in Table 4, along with their statistical uncertainties. During the analysis, we systematically checked all possible variants of signs for the principle transition moment parameters. The number of statistically determined terms (22) is much less than the number of measurements (874). The ratio of the number of fitted intensities over the number of adjusted parameters (38) is 2.1 times the corresponding ratio for the line positions modeling, as seen in Table 2.

Detailed statistics of the intensity fit are given by band in Table 5. As for the position analysis, the main difficulty for the intensity analysis follows from subtle interactions with bands too weak to be seen in our present spectra (originally recorded for the Nonad study). It is clear that transition moments for tertiary bands like $2\nu_3 + \nu_6$ and $\nu_5 + 2\nu_6$ should be small; nevertheless these states could alter the line intensities of bands in the 3500–3700 cm^{-1} region, especially for states whose eigenvectors contain considerable mixtures of $2\nu_3 + \nu_6$ or $\nu_5 + 2\nu_6$. The intensity analysis of the weak bands such as $\nu_3 + 2\nu_6$ (E) and $3\nu_6$ (A_2) is more difficult because we have observed so few lines and the measurement accuracy is poor.

The integrated intensities for the eight components of the Enneadecad are also shown in Table 5, along with estimated hotband values. These have been obtained by summation of the line intensities greater than 10^{-25} ($\text{cm}^{-1}/\text{molecule} \cdot \text{cm}^{-2}$) at 296 K for the number of calculated lines indicated. The bands strengths quoted in Table 5 are essentially governed by purely vibrational transition moments ($R0(0,0A_1)$ type terms) given in Table 4. As expected, the two quanta bands are much stronger than the three quanta bands. The model accuracy is better for the stronger and more isolated bands $\nu_2 + \nu_3$ and $\nu_2 + \nu_6$; thus the summations of calculated intensities for these two bands are more reliable since a few hundred transitions have been modeled. In contrast, the summations could be off by an order of magnitude for bands with less than 10 observed intensities. The $3\nu_6$ (A_2) band is nominally not infrared active, but it apparently borrows intensity from other bands to become stronger than $3\nu_6$ (A_1).

5 Database of line parameters

For terrestrial and planetary remote sensing, a prediction of over 7000 line positions, intensities and lower state transition energies was written into HITRAN [18] database format. The new list covered the region between 3170 and 3700 cm^{-1} and included allowed and forbidden transitions up to $J = 18$. Air- and self-broadened half-widths in $\text{cm}^{-1}/\text{atm}$ were added using empirical expressions obtained in Triad studies (see Refs. [19] and [20] for details). For most transitions, the expression used was:

$$width_{air} = 0.0677 - 5.681 \times 10^{-5}m - 8.397 \times 10^{-5}k^2$$

$$width_{self} = 0.0869 - 6.41 \times 10^{-5}m - 6.56 \times 10^{-5}k^2$$

where m is J'' for P and Q branch transitions and $J + 1$ for R branch lines; k = lower state K for $\Delta K = -1$ and 0 and k = upper state K for $\Delta K = +1$. However, a different expression was required for transitions with $J'' = K''$ for $^P P$, $^Q Q$, $^R R$ lines:

$$width_{air} = 0.06863 - 3.762 \times 10^{-4}m + 7.044 \times 10^{-7}m^2$$

$$width_{self} = 0.0875 - 3.46 \times 10^{-4}m + 4.94 \times 10^{-7}m^2$$

An estimated pressure-induced frequency shift δ in $\text{cm}^{-1}/\text{atm}$ was computed as $\delta = -0.0025\nu_i/1300$, where ν_i is the line position. The temperature dependence of the air-broadened widths was set to a constant of 0.75. These lists have been submitted for inclusion in the next updates of the HITRAN [18] and GEISA [21] databases.

For astronomy, a separate version is available (from the last author) with the air-broadened widths replaced by H2-

broadening based on the results of Boussin et al. [22] for $3\nu_2$. A synthetic spectrum is shown in Fig. 6. Significantly, the present study reveals that features of CH_3D overlap those of the NH_3 fundamentals near 3330 cm^{-1} [23] and also important bands of PH_3 [24]. Thus, this new CH_3D database is essential for atmospheric studies of the outer planets and Titan.

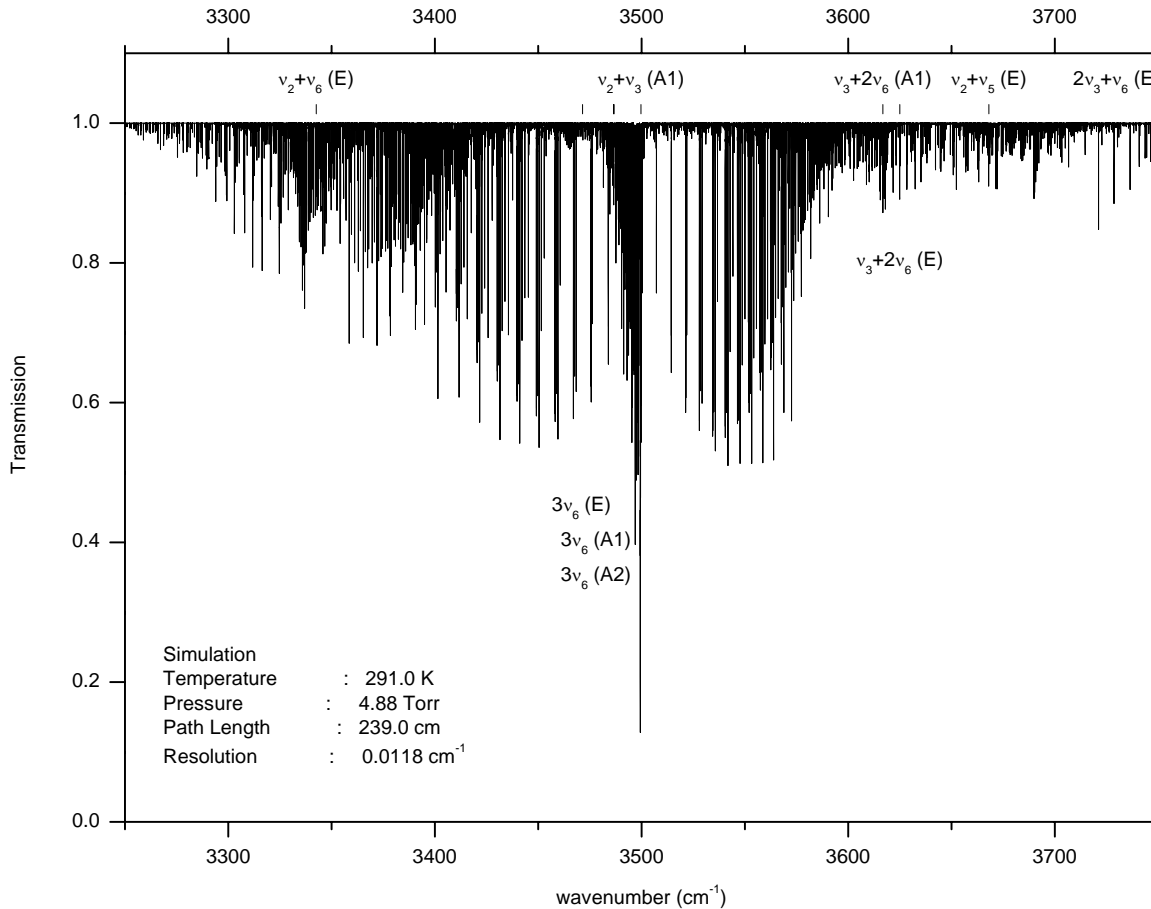


Figure 6: Simulated absorption spectrum of CH_3D in the Lower Enneadecad region.

6 Conclusion

The present analysis represents the first step toward interpreting the higher polyads above the fundamental regions of CH_3D . Here, the available data between 3250 and 3700 cm^{-1} have been used successfully to model 2852 observed positions and 874 line intensities with RMS values of 0.0009 cm^{-1} and 4.6%, respectively. Some hot bands at longer wavelength have also been assigned. This initial progress provides spectroscopic information required for the interpretation of astronomical data by initiating a database of over 7000 CH_3D transitions between 3170 and 3700 cm^{-1} . A similar preliminary analysis of many of the upper 10 bands between 4000 and 4700 cm^{-1} could be pursued immediately with the present data, but the upper portion of the Enneadecad is less important for planetary astronomy because the methane Octad dominates that region. In any case, for further study, the new spectra recorded at longer path lengths are needed to identify many of the 37 vibrational sub-components of the Enneadecad. The results of the simultaneous analysis of the intensities of the Nonad and Enneadecad–Nonad systems will be reported separately.

Acknowledgments

The support of CNRS (France)-RFBR(Russia) through the PICS exchange program 05-05-22001a is acknowledged. The support of RFBR(Russia) through the Grant 06-05-65010a is acknowledged. Most of the research at the Labo-

ratoire de Physique de l'Université de Bourgogne (LPUB) was supported in the framework of the French Programme National de Chimie Atmosphérique. Support from the Region Bourgogne is gratefully acknowledged for computer equipment at the University of Burgundy Physics Laboratory. Part of the research was performed at the Jet Propulsion Laboratory (JPL), California Institute of Technology, under contract with The National Aeronautics and Space Administration. Finally, L.R. Brown wishes to thank S.J. Kim for pointing out the need for the CH₃D database in this region.

References

- [1] T. Encrenaz, *Earth Moon Planets* 67 (1995), pp. 77–87.
- [2] E. Lellouch, B. Bezdard, T. Fouchet, H. Feuchtgruber, T. Encrenaz and T. de Graauw, *Astro. Astrophys.* 370 (2001), pp. 610–622.
- [3] T.R. Geballe, S.J. Kim, K.S. Noll and C.A. Griffith, *Apt. J.* 583 (Pt. 2) (2003), pp. L39–L42.
- [4] R.H. Brown, K.H. Baines, G. Bellucci, B.J. Buratti, F. Capaccioni, P. Cerroni, R.N. Clark, A. Coradini, D.P. Cruikshank, P. Drossart, V. Formisano, R. Jaumann, Y. Langevin, D.L. Matson, T.B. McCord, V. Mennella, R.M. Nelson, P.D. Nicholson, B. Sicardy, C. Sotin, N. Baugh, C.A. Griffith, G.B. Hansen, C.A. Hibbitts, T.W. Momary and M.R. Showalter, *Astro. Astrophys.* 446 (2006), pp. 707–716.
- [5] E.E. Becklin, *IR/Submm. Astron. Space Adv. Space Res.* 36 (2005), pp. 1087–1090.
- [6] S.J. Kim, T.R. Geballe, K.S. Noll and R. Courtin, *Icarus* 173 (2005), pp. 522–532.
- [7] A. Nikitin, J.P. Champion and Vl.G. Tyuterev, *J. Mol. Spectrosc.* 182 (1997), pp. 72–84.
- [8] A. Nikitin, J.P. Champion and Vl.G. Tyuterev, *J. Quant. Spectrosc. Rad. Transfer* 82 (2003), pp. 239–249.
- [9] J.P. Champion, *Can. J. Phys.* 55 (1977), pp. 1802–1828.
- [10] J.P. Champion, M. Loete and G. Pierre, Spherical top spectra. In: K.N. Rao and A. Weber, Editors, *Spectroscopy of the Earth's Atmosphere and Interstellar Medium*, Academic Press, Boston, Ma (1992), pp. 97–151 (Chapter 2).
- [11] A. Nikitin, J.P. Champion, Vl.G. Tyuterev, L.R. Brown, G. Mellau and M. Lock, *J. Mol. Struct.* 517–518 (2000), pp. 1–24.
- [12] A. Nikitin, L.R. Brown, L. Fejard, J.P. Champion and Vl.G. Tyuterev, *J. Mol. Spectrosc.* 216 (2002), pp. 225–251.
- [13] J.C. Hilico, O. Robert, M. Loete, S. Toumi, A.S. Pine and L.R. Brown, *J. Mol. Spectrosc.* 208 (2001), pp. 1–13.
- [14] L.R. Brown, J.S. Margolis, R.H. Norton and B.D. Stedry, *Appl. Spectrosc.* 37 (1983), pp. 287–292.
- [15] A.G. Maki, J.S. Wells, *Wavenumber Calibration tables from heterodyne frequency measurements*, NIST Special Publication 821 US Government Printing Office, 1991.
- [16] A. Predoi-Cross, K. Hambrook, M. Brawley-Tremblay, J.-P. Bouanich, V. Malathy Devi, D. Chris Benner and L.R. Brown, *J. Mol. Spectrosc.* 234 (2005), pp. 53–74.
- [17] O.N. Ulenikov, G.A. Onopenko, N.E. Tyabaeva, R. Anttila, S. Alanko and J. Schroderus, *J. Mol. Spectrosc.* 193 (1999), pp. 249–259.
- [18] L.S. Rothman, D. Jacquemart, A. Barbe, D.C. Benner, M. Birk, L.R. Brown, M.R. Carleer, C. Chackerian Jr., K. Chance, V. Dana, V.M. Devi, J.-M. Flaud, R.R. Gamache, J.-M. Hartmann, K.W. Jucks, A.G. Maki, J.-Y. Mandin, S. Massie, J. Orphal, A. Perrin, C.P. Rinsland, M.A.H. Smith, R.A. Toth, J. Vander Auwera, P. Varanasi and G. Wagner, *J. Quant. Spectrosc. Rad. Transfer* 96 (2005), pp. 139–204.

- [19] L.R. Brown, D.C. Benner, J.P. Champion, V.M. Devi, L. Fejard, R.R. Gamache, T. Gabard, J.C. Hilico, B. Lavorel, M. Loëte, G.C. Mellau, A. Nikitin, A.S. Pine, A. Predoi-Cross, C.P. Rinsland, O. Robert, R.L. Sams, M.A.H. Smith, S.A. Tashkun and Vl.G. Tyuterev, *J. Quant. Spectrosc. Rad. Transfer* 82 (2003), pp. 219–238.
- [20] V.M. Devi, D.C. Benner, M.A.H. Smith and C.P. Rinsland, *J. Quant. Spectrosc. Rad. Transfer* 68 (2001), pp. 135–161.
- [21] N. Jacquinet-Husson, N.A. Scott, A. Chédin, K. Garceran, R. Armante, A.A. Chursin, A. Barbe, M. Birk, L.R. Brown, C. Camy-Peyret, C. Claveau, C. Clerbaux, P.F. Coheur, V. Dana, L. Daumont, M.R. Debacker-Barilly, J.M. Flaud, A. Goldman, A. Hamdouni, M. Hess, K. Köpke, J.Y. Mandin, S. Massie, S. Mikhailenko, V. Nemtchinov, A. Nikitin, D. Newnham, A. Perrin, V.I. Perevalov, L. Régalia-Jarlot, A. Rublev, F. Schreier, L. Schult, K.M. Smith, S.A. Tashkun, J.L. Teffo, R.A. Toth, Vl.G. Tyuterev, J. Vander-Auwer, P. Varanasi and G. Wagner, *J. Quant. Spectrosc. Rad. Transfer* 95 (2005), pp. 429–467.
- [22] C. Boussin, B.L. Lutz, A. Hamdouni and C. de Bergh, *J. Quant. Spectrosc. Rad. Transfer* 63 (1999), pp. 49–84.
- [23] I. Kleiner, G. Tarrago, C. Cottaz, L. Sagui, L.R. Brown, R.L. Poynter, H.M. Pickett, P. Chen, J.C. Pearson, R.L. Sams, G.A. Blake, S. Matsuura, V. Nemtchinov, P. Varanasi, L. Fusina and G. Di Lonardo, *J. Quant. Spectrosc. Rad. Transfer* 82 (2003), pp. 293–312.
- [24] R.A.H. Butler, L. Sagui, I. Kleiner and L.R. Brown, *J. Mol. Spectrosc.* 238 (2006), pp. 178–192.

Appendix A. Effective Hamiltonian Terms for the Enneadecad $^{12}\text{CH}_3\text{D}$

	Tensorial nomenclature		Parameter value	
	Rotational	Vibrational	Computer input	Rounded (St.Dev.)
1	R0(0,0A1)	011000 011000	-3.1611633317	-3.161(95)
2	R2(2,0A1)	011000 011000	$-8.6508329946 \times 10^{-3}$	$-8.650(99) \times 10^{-3}$
3	R4(0,0A1)	011000 011000	$4.1173110580 \times 10^{-5}$	$4.11(14) \times 10^{-5}$
4	R4(2,0A1)	011000 011000	$3.5351905252 \times 10^{-6}$	$3.53(19) \times 10^{-6}$
5	R1(1,1E)	011000 010010	$7.8632909060 \times 10^{-2}$	$7.86(28) \times 10^{-2}$
6	R2(2,1E)	011000 010010	$6.6579393473 \times 10^{-2}$	$6.657(87) \times 10^{-2}$
7	R2(2,2E)	011000 010010	$5.7401442498 \times 10^{-2}$	$5.74(10) \times 10^{-2}$
8	R3(1,1E)	011000 010010	$5.4138286884 \times 10^{-4}$	$5.41(17) \times 10^{-4}$
9	R3(3,1E)	011000 010010	$-5.7621361901 \times 10^{-4}$	$-5.76(11) \times 10^{-4}$
10	R3(3,2E)	011000 010010	$-5.9037225687 \times 10^{-4}$	$-5.90(26) \times 10^{-4}$
11	R4(2,1E)	011000 010010	$1.3439146284 \times 10^{-5}$	$1.343(49) \times 10^{-5}$
12	R4(4,1E)	011000 010010	$-2.1556963781 \times 10^{-6}$	$-2.15(26) \times 10^{-6}$
13	R4(4,4E)	011000 010010	$3.7215976177 \times 10^{-6}$	$3.72(23) \times 10^{-6}$
14	R1(1,1E)	011000 010001	$-7.8470035328 \times 10^{-1}$	$-7.84(13) \times 10^{-1}$
15	R2(2,1E)	011000 010001	$2.6121105537 \times 10^{-2}$	$2.61(10) \times 10^{-2}$
16	R2(2,2E)	011000 010001	$1.8607166659 \times 10^{-2}$	$1.860(66) \times 10^{-2}$
17	R3(3,1E)	011000 010001	$3.0939985620 \times 10^{-4}$	$3.09(12) \times 10^{-4}$
18	R3(3,2E)	011000 010001	$4.7862996020 \times 10^{-4}$	$4.78(20) \times 10^{-4}$
19	R4(2,1E)	011000 010001	$7.4486158966 \times 10^{-6}$	$7.44(32) \times 10^{-6}$
20	R4(2,2E)	011000 010001	$4.1192550179 \times 10^{-6}$	$4.11(42) \times 10^{-6}$
21	R4(4,1E)	011000 010001	$-8.5431868971 \times 10^{-6}$	$-8.54(32) \times 10^{-6}$
22	R1(1,1E)	011000 001002	$5.6559598222 \times 10^{-1}$	$5.65(15) \times 10^{-1}$
23	R2(2,1E)	011000 001002	$-5.1166682839 \times 10^{-3}$	$-5.11(81) \times 10^{-3}$
24	R2(2,2E)	011000 001002	$-1.2283621540 \times 10^{-2}$	$-1.228(44) \times 10^{-2}$
25	R3(1,1E)	011000 001002	$2.8670954119 \times 10^{-4}$	$2.86(11) \times 10^{-4}$
26	R3(3,1E)	011000 001002	$-3.5650200056 \times 10^{-4}$	$-3.56(17) \times 10^{-4}$
27	R3(3,2E)	011000 001002	$8.9190287151 \times 10^{-4}$	$8.91(13) \times 10^{-4}$
28	R0(0,0A1)	011000 001002	-21.370923009	-21.37(24)
29	R2(0,0A1)	011000 001002	$-2.8574422120 \times 10^{-3}$	$-2.85(12) \times 10^{-3}$
30	R3(3,3A1)	011000 001002	$-1.3025088991 \times 10^{-4}$	$-1.302(54) \times 10^{-4}$
31	R1(1,0A2)	011000 000003	$-1.7974869387 \times 10^{-1}$	$-1.797(42) \times 10^{-1}$
32	R3(1,0A2)	011000 000003	$9.9509780659 \times 10^{-5}$	$9.9(10) \times 10^{-5}$
33	R3(3,3A2)	011000 000003	$5.3031425818 \times 10^{-5}$	$5.30(38) \times 10^{-5}$
34	R0(0,0A1)	011000 000003	$-6.3120603421 \times 10^{-1}$	$-6.312(61) \times 10^{-1}$
35	R2(0,0A1)	011000 000003	$1.0320254709 \times 10^{-3}$	$1.03(12) \times 10^{-3}$
36	R1(1,1E)	011000 000003	$-5.6094981036 \times 10^{-1}$	$-5.609(97) \times 10^{-1}$
37	R2(2,1E)	011000 000003	$-1.0847381515 \times 10^{-2}$	$-1.084(31) \times 10^{-2}$
38	R2(2,2E)	011000 000003	$-3.9424714003 \times 10^{-3}$	$-3.94(12) \times 10^{-3}$
39	R3(3,1E)	011000 000003	$1.9215581838 \times 10^{-4}$	$1.921(46) \times 10^{-4}$
40	R3(3,2E)	011000 000003	$1.7006047650 \times 10^{-4}$	$1.70(10) \times 10^{-4}$
41	R0(0,0A1)	010010 010010	-6.2926869242	-6.292(16)
42	R1(1,0A2)	010010 010010	$1.3106131910 \times 10^{-1}$	$1.310(18) \times 10^{-1}$
43	R2(0,0A1)	010010 010010	$8.4674126965 \times 10^{-3}$	$8.467(86) \times 10^{-3}$
44	R2(2,0A1)	010010 010010	$-3.7746802870 \times 10^{-3}$	$-3.774(95) \times 10^{-3}$

	Tensorial nomenclature		Parameter value	
	Rotational	Vibrational	Computer input	Rounded (St.Dev.)
45	R2(2,1E)	010010 010010	$1.0965233352 \times 10^{-2}$	$1.09(11) \times 10^{-2}$
46	R3(1,0A2)	010010 010010	$7.4517451335 \times 10^{-4}$	$7.45(20) \times 10^{-4}$
47	R3(3,0A2)	010010 010010	$6.6977460240 \times 10^{-4}$	$6.69(18) \times 10^{-4}$
48	R3(3,3A2)	010010 010010	$3.4073737750 \times 10^{-4}$	$3.40(25) \times 10^{-4}$
49	R4(0,0A1)	010010 010010	$-5.8578839279 \times 10^{-5}$	$-5.85(14) \times 10^{-5}$
50	R4(2,0A1)	010010 010010	$-4.0917824781 \times 10^{-6}$	$-4.09(15) \times 10^{-6}$
51	R4(2,1E)	010010 010010	$8.7693219011 \times 10^{-6}$	$8.76(74) \times 10^{-6}$
52	R4(2,2E)	010010 010010	$1.4254998661 \times 10^{-5}$	$1.425(73) \times 10^{-5}$
53	R4(4,0A1)	010010 010010	$6.1600889069 \times 10^{-6}$	$6.16(16) \times 10^{-6}$
54	R4(4,1E)	010010 010010	$4.1059955688 \times 10^{-6}$	$4.10(43) \times 10^{-6}$
55	R4(4,2E)	010010 010010	$-2.9432145986 \times 10^{-5}$	$-2.943(60) \times 10^{-5}$
56	R4(4,4E)	010010 010010	$7.8950869015 \times 10^{-6}$	$7.89(42) \times 10^{-6}$
57	R0(0,0A1)	010010 010001	18.032966855	18.03(20)
58	R1(1,1E)	010010 010001	-2.7615428393	-2.761(39)
59	R2(0,0A1)	010010 010001	$-1.3610546806 \times 10^{-2}$	$-1.361(45) \times 10^{-2}$
60	R2(2,0A1)	010010 010001	$-2.3150507335 \times 10^{-2}$	$-2.315(38) \times 10^{-2}$
61	R2(2,1E)	010010 010001	$-7.7548230555 \times 10^{-2}$	$-7.75(19) \times 10^{-2}$
62	R3(3,3A1)	010010 010001	$3.5457328207 \times 10^{-4}$	$3.545(98) \times 10^{-4}$
63	R3(3,3A2)	010010 010001	$3.2192514009 \times 10^{-4}$	$3.21(11) \times 10^{-4}$
64	R3(3,1E)	010010 010001	$-3.0283402877 \times 10^{-4}$	$-3.02(22) \times 10^{-4}$
65	R0(0,0A1)	010010 002001	-4.7737768659	-4.773(27)
66	R1(1,1E)	010010 002001	$2.5830873598 \times 10^{-1}$	$2.583(89) \times 10^{-1}$
67	R0(0,0A1)	010010 001002	3.6003602792	3.600(51)
68	R1(1,0A2)	010010 001002	$1.0501821412 \times 10^{-1}$	$1.050(48) \times 10^{-1}$
69	R1(1,1E)	010010 001002	$2.6206457773 \times 10^{-1}$	$2.620(59) \times 10^{-1}$
70	R2(0,0A1)	010010 001002	$-1.0321460277 \times 10^{-3}$	$-1.03(16) \times 10^{-3}$
71	R2(2,0A1)	010010 001002	$1.0518316156 \times 10^{-2}$	$1.051(32) \times 10^{-2}$
72	R2(2,1E)	010010 001002	$-2.8062696123 \times 10^{-2}$	$-2.806(33) \times 10^{-2}$
73	R2(2,2E)	010010 001002	$-7.7097511379 \times 10^{-3}$	$-7.70(23) \times 10^{-3}$
74	R3(1,1E)	010010 001002	$-1.8797995290 \times 10^{-4}$	$-1.87(10) \times 10^{-4}$
75	R3(3,3A1)	010010 001002	$-1.7662701390 \times 10^{-4}$	$-1.766(71) \times 10^{-4}$
76	R3(3,3A2)	010010 001002	$-1.1334778650 \times 10^{-4}$	$-1.133(76) \times 10^{-4}$
77	R3(3,1E)	010010 001002	$4.9413790714 \times 10^{-4}$	$4.94(20) \times 10^{-4}$
78	R3(3,2E)	010010 001002	$-2.8156242288 \times 10^{-4}$	$-2.815(99) \times 10^{-4}$
79	R1(1,1E)	010010 001002	$4.1391159569 \times 10^{-1}$	$4.139(61) \times 10^{-1}$
80	R2(2,1E)	010010 001002	$-7.5127702395 \times 10^{-3}$	$-7.51(32) \times 10^{-3}$
81	R3(1,1E)	010010 001002	$8.5878273303 \times 10^{-5}$	$8.5(12) \times 10^{-5}$
82	R3(3,2E)	010010 001002	$-1.7301695765 \times 10^{-4}$	$-1.73(16) \times 10^{-4}$
83	R0(0,0A1)	010001 010001	-22.912310397	22.912(57)
84	R2(2,0A1)	010001 010001	$6.8671884907 \times 10^{-3}$	$6.867(70) \times 10^{-3}$
85	R2(2,1E)	010001 010001	$3.6536118421 \times 10^{-2}$	$3.65(10) \times 10^{-2}$
86	R2(2,2E)	010001 010001	$1.2632607915 \times 10^{-2}$	$1.263(14) \times 10^{-2}$
87	R4(0,0A1)	010001 010001	$4.0115618392 \times 10^{-5}$	$4.01(11) \times 10^{-5}$
88	R4(4,0A1)	010001 010001	$-3.9342280747 \times 10^{-6}$	$-3.93(16) \times 10^{-6}$
89	R4(4,3A1)	010001 010001	$-1.6610048714 \times 10^{-5}$	$-1.661(34) \times 10^{-5}$
90	R0(0,0A1)	010001 001002	-18.947046472	-18.94(22)

	Tensorial nomenclature		Parameter value	
	Rotational	Vibrational	Computer input	Rounded (St.Dev.)
91	R1(1,0A2)	010001 001002	-1.0206043190	-1.020(13)
92	R1(1,1E)	010001 001002	1.7633175882	1.763(17)
93	R2(2,0A1)	010001 001002	$5.2573406400 \times 10^{-3}$	$5.25(28) \times 10^{-3}$
94	R2(2,1E)	010001 001002	$-1.8415826008 \times 10^{-2}$	$-1.841(55) \times 10^{-2}$
95	R3(1,0A2)	010001 001002	$-1.5654875574 \times 10^{-4}$	$-1.565(78) \times 10^{-4}$
96	R3(1,1E)	010001 001002	$-2.1274318860 \times 10^{-4}$	$-2.127(83) \times 10^{-4}$
97	R3(3,3A1)	010001 001002	$-5.1574089388 \times 10^{-5}$	$-5.15(60) \times 10^{-5}$
98	R3(3,0A2)	010001 001002	$3.1494386723 \times 10^{-4}$	$3.149(57) \times 10^{-4}$
99	R3(3,1E)	010001 001002	$3.1068153695 \times 10^{-4}$	$3.106(96) \times 10^{-4}$
100	R3(3,2E)	010001 001002	$1.9554580049 \times 10^{-4}$	$1.95(14) \times 10^{-4}$
101	R1(1,1E)	010001 001002	-1.6724797686	-1.672(19)
102	R2(2,1E)	010001 001002	$-1.8730019705 \times 10^{-2}$	$-1.873(46) \times 10^{-2}$
103	R2(2,2E)	010001 001002	$-8.6452376685 \times 10^{-3}$	$-8.64(62) \times 10^{-3}$
104	R3(1,1E)	010001 001002	$-1.8205249271 \times 10^{-4}$	$-1.82(10) \times 10^{-4}$
105	R3(3,1E)	010001 001002	$1.0708720996 \times 10^{-4}$	$1.070(93) \times 10^{-4}$
106	R3(3,2E)	010001 001002	$4.6495317591 \times 10^{-4}$	$4.64(17) \times 10^{-4}$
107	R1(1,1E)	010001 000003	$4.3562410162 \times 10^{-1}$	$4.356(92) \times 10^{-1}$
108	R2(2,1E)	010001 000003	$2.9952037483 \times 10^{-2}$	$2.995(30) \times 10^{-2}$
109	R2(2,2E)	010001 000003	$-2.0867481499 \times 10^{-2}$	$-2.086(25) \times 10^{-2}$
110	R3(1,1E)	010001 000003	$-9.5051306918 \times 10^{-5}$	$-9.50(60) \times 10^{-5}$
111	R3(3,2E)	010001 000003	$2.6357764873 \times 10^{-4}$	$2.63(12) \times 10^{-4}$
112	R1(1,1E)	010001 000003	$3.0615556160 \times 10^{-1}$	$3.061(75) \times 10^{-1}$
113	R2(2,1E)	010001 000003	$2.3207699492 \times 10^{-2}$	$2.320(37) \times 10^{-2}$
114	R2(2,2E)	010001 000003	$1.5622358608 \times 10^{-2}$	$1.562(28) \times 10^{-2}$
115	R3(1,1E)	010001 000003	$9.2178094198 \times 10^{-5}$	$9.21(66) \times 10^{-5}$
116	R3(3,2E)	010001 000003	$2.3885413695 \times 10^{-4}$	$2.38(12) \times 10^{-4}$
117	R0(0,0A1)	010001 000003	17.653139938	17.65(28)
118	R1(1,0A2)	010001 000003	$1.2103156184 \times 10^{-1}$	$1.210(19) \times 10^{-1}$
119	R2(0,0A1)	010001 000003	$-2.1219324381 \times 10^{-3}$	$-2.12(13) \times 10^{-3}$
120	R2(2,0A1)	010001 000003	$-1.9797648041 \times 10^{-3}$	$-1.97(10) \times 10^{-3}$
121	R2(2,1E)	010001 000003	$-1.2295112335 \times 10^{-2}$	$-1.229(18) \times 10^{-2}$
122	R2(2,2E)	010001 000003	$-1.0496006684 \times 10^{-2}$	$-1.049(21) \times 10^{-2}$
123	R3(1,0A2)	010001 000003	$1.1352640020 \times 10^{-4}$	$1.135(37) \times 10^{-4}$
124	R3(3,3A1)	010001 000003	$1.7632910791 \times 10^{-4}$	$1.763(70) \times 10^{-4}$
125	R3(3,3A2)	010001 000003	$7.8785418351 \times 10^{-5}$	$7.87(45) \times 10^{-5}$
126	R3(3,1E)	010001 000003	$2.1273008304 \times 10^{-4}$	$2.127(64) \times 10^{-4}$
127	R0(0,0A1)	001002 001002	-1.0033924244	-1.003(23)
128	R1(1,0A2)	001002 001002	$-7.8043747608 \times 10^{-2}$	$-7.80(19) \times 10^{-2}$
129	R2(0,0A1)	001002 001002	$-2.7151429010 \times 10^{-3}$	$-2.71(11) \times 10^{-3}$
130	R2(2,1E)	001002 001002	$-4.0393784254 \times 10^{-2}$	$-4.039(57) \times 10^{-2}$
131	R2(2,2E)	001002 001002	$5.6234004121 \times 10^{-4}$	$5.62(41) \times 10^{-4}$
132	R1(1,1E)	001002 001002	$-1.6284466999 \times 10^{-1}$	$-1.628(28) \times 10^{-1}$
133	R2(2,2E)	001002 001002	$-3.2633853190 \times 10^{-3}$	$-3.26(10) \times 10^{-3}$
134	R0(0,0A1)	001002 001002	-5.2870886079	-5.287(95)
135	R2(0,0A1)	001002 001002	$-7.0161653250 \times 10^{-3}$	$-7.01(18) \times 10^{-3}$
136	R2(2,0A1)	001002 001002	$8.0563091249 \times 10^{-3}$	$8.056(89) \times 10^{-3}$

	Tensorial nomenclature		Parameter value	
	Rotational	Vibrational	Computer input	Rounded (St.Dev.)
137	R0(0,0A1)	000003 000003	$1.3965965255 \times 10^{-1}$	$1.3965(65) \times 10^{-1}$
138	R2(0,0A1)	000003 000003	$-5.9659906675 \times 10^{-3}$	$-5.96(10) \times 10^{-3}$
139	R1(1,1E)	000003 000003	$-7.0272217310 \times 10^{-2}$	$-7.02(14) \times 10^{-2}$
140	R2(2,1E)	000003 000003	$1.6520371364 \times 10^{-2}$	$1.652(29) \times 10^{-2}$
141	R2(2,2E)	000003 000003	$-6.5780459466 \times 10^{-4}$	$-6.57(35) \times 10^{-4}$
142	R1(1,0A2)	000003 000003	$-2.9857615583 \times 10^{-3}$	$-2.985(91) \times 10^{-3}$
143	R0(0,0A1)	000003 000003	$-9.9095395364 \times 10^{-2}$	$-9.909(93) \times 10^{-2}$
144	R2(0,0A1)	000003 000003	$2.4977485850 \times 10^{-3}$	$2.497(47) \times 10^{-3}$
145	R2(2,0A1)	000003 000003	$1.5530171952 \times 10^{-3}$	$1.553(29) \times 10^{-3}$
146	R1(1,1E)	000003 000003	$3.5624914150 \times 10^{-2}$	$3.56(16) \times 10^{-2}$
147	R2(2,1E)	000003 000003	$7.2910732950 \times 10^{-3}$	$7.29(21) \times 10^{-3}$
148	R2(2,2E)	000003 000003	$-1.3438465775 \times 10^{-3}$	$-1.343(29) \times 10^{-3}$
149	R0(0,0A1)	000003 000003	-3.2293910792	-3.229(56)
150	R2(0,0A1)	000003 000003	$-1.9155050804 \times 10^{-3}$	$-1.915(53) \times 10^{-3}$
151	R2(2,0A1)	000003 000003	$-2.4103810728 \times 10^{-3}$	$-2.410(54) \times 10^{-3}$
152	R2(2,1E)	000003 000003	$1.5629603704 \times 10^{-2}$	$1.562(25) \times 10^{-2}$
153	R2(2,2E)	000003 000003	$-1.4895183238 \times 10^{-3}$	$-1.489(68) \times 10^{-3}$